J Solid State Electrochem (2007) 11:703–710
DOI 10.1007/s10008-006-0237-5

ORIGINAL PAPER

Electrochemical characterization of Ni–Fe alloy codeposition under MHD control

J.-P. Chopart · O. Aaboubi · K. Msellak

Received: 19 May 2006 / Accepted: 26 October 2006 / Published online: 16 January 2007

Abstract The nickel–iron alloy electrodeposition is affected by a superimposed magnetic field. Some previous papers [Msellak et al., Magnetohydrodynamics, 39:487–493, 2003 and Msellak et al., J Magn Magn Mat, 281:295–304, 2004] have exhibited some dramatic changes in iron amount and morphology of these deposits. As it is usual for a magnetic field up to 1 T, no charge transfer effect can be expected, and the observed modifications can be explained by the magnetohydrodynamic convection that controls the iron species flux during the electrochemical reaction. By electrochemical impedance spectroscopy and physical investigations (scanning electron microscopy, X-ray diffraction, and inductively coupled plasma), the reduction process is analyzed, the characteristic parameters of the mechanism are determined, and the magnetic field effects can be quantified.

Keywords Iron–nickel alloy · Electrodeposition · Magnetohydrodynamics · Electrochemical impedance spectroscopy

Introduction

In two previous papers [1, 2], we have undertaken the analyses of magnetic field effects on Ni–Fe alloy electrodeposition. For the experimental conditions that have been chosen, the induced magnetic convection dramatically changed the surface morphology and the iron amount of the deposited alloys. These results are in accordance with previous papers on classical magnetohydrodynamical (MHD) effects that increase the surface concentration of electrochemical species that are under diffusion control [3, 4]. For the anomalous Ni–Fe codeposition that has been largely investigated [5–11], a mechanism model has been developed by Matlosz [10] and confirmed by electrochemical impedance spectroscopy (EIS) measurements [11]. In this model, $Ni(I)_{ads}$ and $Fe(I)_{ads}$ species compete for adsorption, and $Fe(OH)^{+}$ acts as an inhibiting species for the nickel electrodeposition. Zech et al. [12, 13] developed a model in which a catalytic step was added to explain the fast reduction of iron species when nickel species are present in the solution. Later, Vaes et al. [14, 15] brought some experimental evidences, which belie the role of the hydroxyl intermediates. In this paper, our goal is to investigate the electrodeposition of the Ni–Fe alloy under MHD conditions by dynamic electrochemical technique (EIS) for determining the characteristic parameters of the electrochemical reactions.

Experimental conditions

Experiments were performed with a classical three-electrode cell that was thermostatically controlled at a constant temperature (25 °C) by circulating water in the double wall of the cell. The cell was put into the gap of an electromagnet (Drusch EAM 20G). The applied magnetic field was uniform and homogeneous onto the whole cell. The working electrode was a 6-mm-diameter downward copper disc that was placed parallel to the horizontal magnetic field. The counter electrode was a platinum grid, and the reference electrode was a saturated mercury sulfate electrode (SSE).

For stationary current–potential curves $I(E)$, before each measurement, a predeposit was made at a constant potential

Contribution to special issue on "Magnetic field effects in Electrochemistry".

J.-P. Chopart (✉) · O. Aaboubi · K. Msellak
Dynamique des Transferts aux Interfaces, EA 3803,
Université de Reims Champagne-Ardenne,
BP 1039, 51687 Reims Cedex 2, France
e-mail: jp.chopart@univ-reims.fr

(E_{appl}=−1.4 V/SSE during 5 min), and the $I(E)$ curve was recorded with a low scan speed (2 mV/s) to be able to assume quasi stationary conditions. E is the actual potential vs the reference electrode potential ($E=E_{appl}-R_S.I$ with E_{appl} as the potential applied between the working electrode and the reference electrode and R_S the electrolytic resistance).

The EIS experiments were performed in a potentiostatic mode by means of an electrochemical interface (Solartron 1286) coupled with a frequency-response analyzer (Solartron 1250). Before each EIS measurement, the working electrode was mechanically polished, using Struers papers of different grades, up to 4,000 and the alloy was electrodeposited at the same constant potential value that was applied for the EIS experiment. This potentiostatic deposition was realized during a sufficient time to get a stationary current. To confirm no surface evolution, the stationary currents before and after the EIS experiment were compared, and data were kept if no current modification was noticed. The low frequency domain (frequency < 10 mHz) was not investigated to avoid the surface and current evolutions. All the experiments were realized at least three times, reproducibility was confirmed, and the average values were used for analyses. The electrolyte was an acidic sulfate solution made with distilled water containing metal ions (from $NiSO_4$, 6 H_2O and Fe SO_4, 7 H_2O) and boric acid. Sodium sulfate was added to keep constant the sulfate concentration. The solution pH was adjusted to 3 with few drops of sulfuric acid. The alloy chemical composition has been determined by means of an absorption atomic spectroscopy analysis (inductively coupled plasma [ICP]) after dissolution of the NiFe deposit by nitric acid solution.

Results and discussion

Stationary mode

Nickel electrodeposition

For a solution without iron ions, the current–potential curves measured with or without a superimposed magnetic field are similar and only a slight increase of the current can be noticed for cathodic potential E up to −1.4 V/SSE (Fig. 1). For more negative potentials, the increase of the current that can be observed is due to the MHD convection that is effective on the hydrogen ion, which reacts under mass transport control. For low overpotential, the nickel ion is not mass-transport controlled, and the charge transfer regime occurs in two Tafel steps:

$$Ni(II)+e^- \rightarrow Ni(I)_{ads} \quad \text{(step 1)}$$

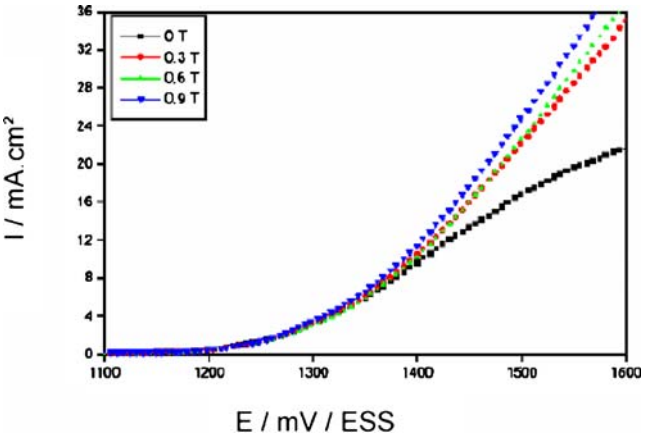

Fig. 1 Current density–potential curves (I vs $-E$) for nickel electrodeposition and different superimposed magnetic fields. $NiSO_4$=0.5 mol l^{-1}, Na_2SO_4=0.6 mol l^{-1}, H_3BO_3=0.4 mol l^{-1}, pH=3, T=25 °C

$$Ni(I)_{ads}+e^- \rightarrow Ni \quad \text{(step 2)}$$

where the subscript ads stands for adsorbed.

Furthermore, the hydrogen reduction current can be regarded as negligible. Therefore, the lack of magnetic effect on the total current is coherent with previous results [16, 17].

For the nickel reduction, according to steps 1 and 2, the total faradic current is given by:

$$I= FA[k_1.C_N.(1-\theta_N)+k_2.\Gamma_N.\theta_N] \quad (1)$$

where F is the Faraday constant, A is the total surface electrode, C_N is the concentration of the reactive Ni(II) species at the electrode surface. θ_N is the fraction of the surface covered by the $Ni(I)_{ads}$ species, and Γ_N is the surface concentration of $Ni(I)_{ads}$ on the adsorbed surface; it is a constant and has a typical value equal to 8×10^{-5} mol m^{-2} [18]. k_1 and k_2 are the rate constants of the two steps, respectively 1 and 2, and they are expressed by:

$$k_i=k_i^0\exp(-b_i.E) \quad (2)$$

in which the pre-exponential term k_i^0 depends on the reference potential and b_i is the corresponding Tafel coefficient in the step i.

For steady state ($d\theta_N/dt$=0), the covered surface ratio θ_{NS} is:

$$\theta_{NS}=k_1.C_N/(k_1.C_N+k_2.\Gamma_N) \quad (3)$$

And, therefore, the total stationary faradic current I_s can be expressed by:

$$I_S= 2FA.[k_1k_2C_N\Gamma_N/(k_1C_N+k_2\Gamma_N)] \quad (4)$$

The logarithmic curves I_S vs E exhibit two slopes (Fig. 2) and two Tafel coefficients b_1 and b_2 can be estimated (Table 1). The first coefficient b_1 does not depend

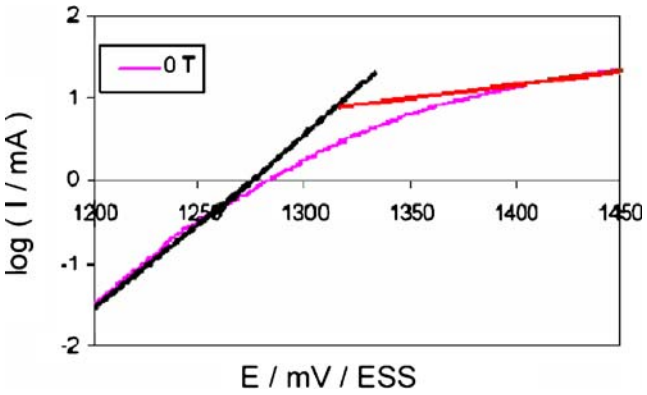

Fig. 2 Semi-logarithmic representation of the current density–potential curves [log(*I*) vs −E]. *B*=0. Same solution as Fig. 1

on the applied magnetic field and the mean value 20 V^{-1} is similar to the Tafel coefficient found by previous workers [11, 18]. The second slope b_2 is determined in a potential zone in which hydrogen reduction is more effective, and an apparent increase of the b_2 coefficient can be noticed. The magneto-induced convection induces two effects in this potential domain: The first one is removing the hydrogen bubbles that germinate on the surface and therefore the electrode surface is not covered by hydrogen, and the actual surface is totally accessible for electrochemical reactions. The second is a classical convective effect, which is very effective for more cathodic applied potentials and leads to the current increase (Fig. 1). Finally, the result for the b_2 coefficient determination under MHD convection is an average value very similar to the value found by Wiart for nickel electrodeposition from Watts bath at a rotating disk electrode. This independence of the Tafel coefficient on magnetic field up to 1 T is completely in accordance with old and recent published results [17, 20, 21]

Nickel–iron electrodeposition

For solution containing iron ion species during the electrodeposition of the alloy, according to Matlosz [10], we may take into account two other reactions which involve the iron species and occur simultaneously with the two nickel steps:

$$Fe(II)+e^- \rightarrow Fe(I)_{ads} \quad \text{(step 3)}$$

$$Fe(I)_{ads}+e^- \rightarrow Fe \quad \text{(step 4)}$$

When hydrogen evolution is negligible and due to the MHD convection, the surface coverage by mass-transport-controlled Fe(II) species is more effective. Therefore, the iron amount in the deposit increases, and because Fe(II) species reaction is slower than Ni(II) reduction, the total current decreases [1, 2].

For an applied potential equal to −1.4 V/SSE, the codeposit analyses by absorption atomic spectroscopy (ICP) exhibit that the hydrogen evolution can be disregarded; therefore, the total current may be expressed as the sum of four terms:

$$I = \mathrm{F}.A(v_1+v_2+v_3+v_4) \quad (5)$$

Where v_i is the rate of the corresponding step. Because iron species are under mass transport control, these rates can be expressed as:

$$v_1 = k_1.C_N(1-\theta_N-\theta_F) \quad (6a)$$

$$v_2 = k_2.\Gamma_N.\theta_N \quad (6b)$$

$$v_3 = (D_F.C_F/\delta)(1-\theta_N-\theta_F) \quad (6c)$$

$$v_4 = k_4.\Gamma_F.\theta_F \quad (6d)$$

where C_F is the bulk solution concentration of Fe(II) species that react at the electrode and δ is the diffusion layer thickness. D_F is the diffusion coefficient of Fe(II) ion and is equal to 4.6×10^{-10} m^2 s^{-1} [10]. Γ_F, θ_F, k_3 and k_4 stand for the classical meaning for the iron species parameters.

At steady state, because $v_1=v_2$ and $v_3=v_4$, the two ratios can be determined and the total current is (by convention the current is positive):

$$I_T = \mathrm{F}A.[(Y_1+k_1C_N)(1-\theta_{NS}-\theta_{FS})+Y_2.\theta_{FS}+k_2.\Gamma_N.\theta_{NS}] \quad (7)$$

where θ_{NS} and θ_{FS} are the covered surface factions in stationary mode and are expressed as:

$$\theta_{FS} = 1/[1+(Y_2/Y_1)(1+k_1C_N/k_2\Gamma_N)] \quad (8a)$$

and

$$\theta_{NS} = 1/[1+(1+Y_1/Y_2).(k_2\Gamma_N/k_1C_N)] \quad (8b)$$

Table 1 Tafel coefficients b_1 and b_2 for nickel system (free iron solution)

B/*T*	b_1/V^{-1}	b_2/V^{-1}	$(b_1+b_2)/V^{-1}$
0	20.4±0.6	3.4±0.1	23.8±0.7
0.3	19.5±0.6	5.8±0.2	25.3±0.8
0.6	19.3±0.6	8.5±0.3	27.8±0.9
0.9	20.5±0.6	8.7±0.3	29.2±0.9

$NiSO_4$=0.5 mol l^{-1}, Na_2SO_4=0.6 mol l^{-1}, H_3BO_3=0.4 mol l^{-1}, pH=3, *T*=25 °C

with

$$Y_1 = D_F.C_F/\delta \quad (8c)$$

and

$$Y_2 = k_4.\Gamma_F \quad (8d)$$

Dynamic analysis

Nickel electrodeposition

The EIS measurements have been carried out during the nickel electrodeposition for different superimposed magnetic fields. Figure 3 shows some impedance diagrams plotted in Nyquist plan for an applied potential $E=-1.4$ V/SSE.

In the high frequency range (frequency ≥ 10 Hz), the electrochemical impedance Z_{HF} is given by [22]:

$$Z_{HF} = RS + [R_{ct}/(1 + R_{ct}.(j\omega)^{\alpha}.Q)] \quad (9)$$

with $j = (-1)^{1/2}$ and ω as the angular frequency ($\omega = 2.\pi.f$, f the frequency in Hertz).

R_{ct} is the charge transfer resistance, Q is the constant phase element that is representative of the double layer phenomenon, and α is an empirical positive constant in the range 0 to 1. When α is equal to 1, Q is entirely identifiable to the double layer capacity C_{dl}. If α is lower than 1, C_{dl} can be expressed according to:

$$C_{dl} = Q^{1/\alpha}.\left(RS^{-1} + R_{ct}^{-1}\right)^{(\alpha-1)/\alpha} \quad (10)$$

Assuming that the mass transport effect is negligible, the derivation of the stationary current (Eq. 4) leads to the faradic impedance Z_F expression:

$$Z_F^{-1} = \Delta I/\Delta E = (\partial I/\partial E)_{\theta_N} + (\partial I/\partial \theta_N)_E(\Delta\theta_N/\Delta E) \quad (11)$$

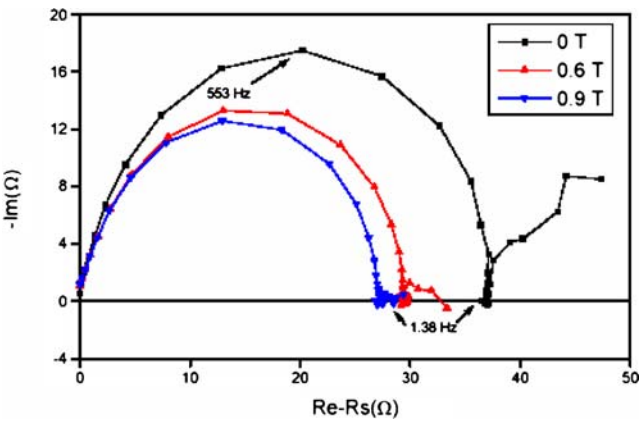

Fig. 3 Nyquist diagrams of EIS data for different magnetic field amplitudes. Same solution as Fig. 1. Applied potential $E=-1.4$ V/SSE

The first term of this expression, which is related to the charge transfer resistance, can be calculated as:

$$(\partial I/\partial E)_{\theta_N} = R_{ct}^{-1} = F A(b_1+b_2)k_1k_2C_N\Gamma_N/(k_1C_N+k_2\Gamma_N) = (b_1+b_2)I_S/2 \quad (12)$$

Therefore, from the experimental high frequency impedances, R_{ct}, R_S, α, Q, and C_{dl} are obtained by matrix regression adjustment. To estimate the accuracy of the calculated parameters and avoid wrong local minimum determination, the calculated parameters are validated by an accurate comparison between experimental and calculated impedance values, frequency for frequency, and the home-made fitting software execute convergence tests. Their values are listed in Table 2 for different superimposed magnetic fields. If the amplitude of the high frequency capacitive loop decreases with the magnetic field, the product of the stationary current I_S and the charge transfer resistance R_{ct} remains constant and equal to 73±2 mV. This fact confirms the magnetic field independence of the kinetic parameters, and we can observe that the other physical terms are not so much modified by magnetic fields. Using the nickel electrodeposition mechanism analysis [19] and the Tafel coefficients b_1 and b_2 obtained by our experimental study, it is possible to calculate the two kinetic constants k_1 and k_2. For an applied potential equal to −1.4 V/SSE, these values are 2.6×10^{-6} m s^{-1} and 16 mol m^{-2} s^{-1}, respectively. These values lead to a resistance charge transfer value of 31 Ω, which is of the same order than the experimental values listed in Table 2, and a concentration C_N of the electroactive Ni(II) species equal to 0.04 mol l^{-1}. This concentration value cannot correspond to a hydroxyl $Ni(OH)^+$ concentration in the electrolyte, which would be much more lower.

Taking into account the equilibrium constant of the $Ni(OH)^+$ formation, which is about 2×10^4 [9] with our pH value equal to 3 and a Ni^{2+} bulk concentration equal to

Table 2 Nickel electrodeposition parameters for free iron species solution

B/ T	R_S/ Ω	α	10^6 Q/IS unit	C_{dl}/ μF	R_{ct}/ Ω	I_s/ mA	$R_{ct}I_s$/ mV	(b_1+b_2)/ V^{-1}
0	15	0.92	56	30	38	1.9	72	28
0.3	12	0.88	99	39	32	2.3	74	27
0.6	12	0.89	83	37	31	2.4	74	27
0.9	13	0.91	71	34	29	2.5	72	28

Same conditions as Table 1. Applied potential $E=-1.4$ V/SSE

R_S Electrolytic resistance, α adimensional term, Q constant phase element, C_{dl} double layer capacity, R_{ct} charge transfer resistance, I_s current, b_1 and b_2 Tafel coefficients

0.5 mol l^{-1}, the $Ni(OH)^{+}$ concentration would be approximately equal to 10^{-7} mol. L^{-1}.

Nickel–iron electrodeposition

In this case, the faradic impedance Z_F' that is obtained by derivation of Eq. 7 is:

$$Z_F'=\left[R_{ct}'^{-1}+B_F.(\Delta\theta_F/\Delta E)+B_N.(\Delta\theta_N/\Delta E)+(\partial I/\partial C_F).(DC_F/DE)\right]^{-1} \quad (13)$$

where R_{ct}' is the new charge transfer resistance:

$$R_{ct}'=1/[FA.(b_2k_2\Gamma_N\theta_{NS}+b_1k_1C_N(1-\theta_{FS}-\theta_{NS})+b_4k_4\Gamma_F\theta_{FS})] \quad (14)$$

and

$$B_F=(\partial I/\partial\theta_F)=FA.[k_1C_N+Y_1-Y_2] \quad (15a)$$

$$B_N=(\partial I/\partial\theta_N)=FA.[k_1C_N-k_2\Gamma_N+Y_1] \quad (15b)$$

$$\Delta\theta_F/\Delta E=\mathrm{Re}(\theta_F)+j.\mathrm{Im}(\theta_F) \quad (15c)$$

$$\Delta\theta_N/\Delta E=\mathrm{Re}(\theta_N)+j.\mathrm{Im}(\theta_N) \quad (15d)$$

in which

$$\mathrm{Re}(\theta_X)=\left[X_1X_3+\omega^2X_2X_4\right]/\left[X_3^2+\omega^2X_4^2\right] \quad (16a)$$

and

$$\mathrm{Im}(\theta_X)=[X_2X_3-X_1X_4]/\left[X_3^2+\omega^2X_4^2\right] \quad (16b)$$

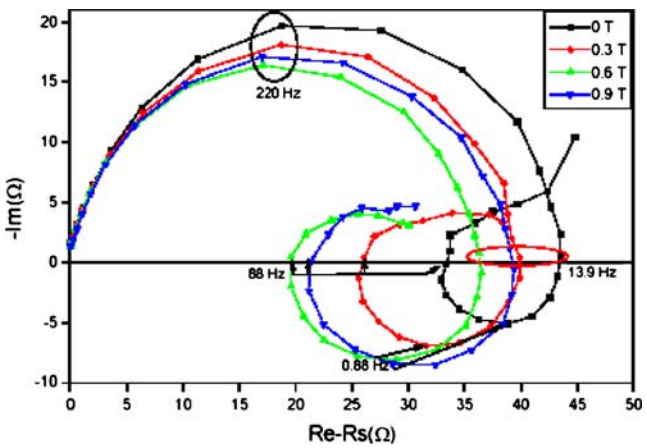

Fig. 4 Nyquist diagrams of EIS data for different magnetic field amplitudes. $NiSO_4$=0.5 mol l^{-1}, $FeSO_4$=0.01 mol l^{-1}, Na_2SO_4=0.6 mol l^{-1}, H_3BO_3=0.4 mol l^{-1}, pH=3, T=25 °C. Applied potential E=−1.4 V/SSE

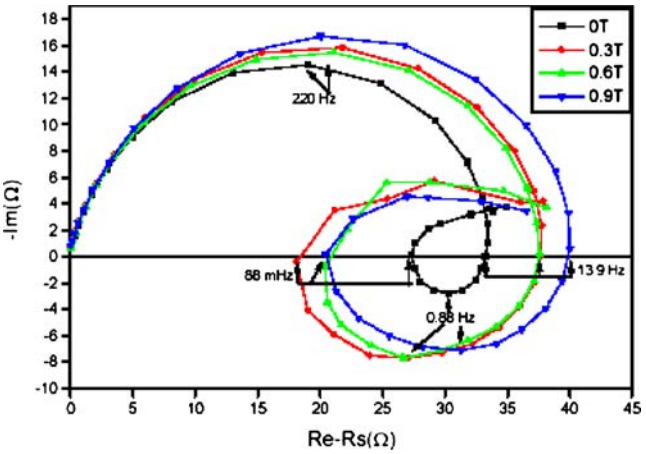

Fig. 5 Nyquist diagrams of EIS data for different magnetic field amplitudes. $NiSO_4$=0.5 mol l^{-1}, $FeSO_4$=0.1 mol l^{-1}, Na_2SO_4=0.6 mol l^{-1}, H_3BO_3=0.4 mol l^{-1}, pH=3, T=25 °C. Applied potential E=−1.4 V/SSE

Where the index X is N for Ni(II) species and F for Fe (II) species. The other parameters used in Eqs. 16a and 16b are defined as:

$$F_1=b_4Y_2\theta_{FS}N_3-Y_1N_1 \quad (17a)$$

$$F_2=b_4Y_2\theta_{FS}N_4-Y_1N_2, \quad (17b)$$

$$F_3=(Y_1+Y_2).N_3-\omega^2N_4\Gamma_F \quad (17c)$$

$$F_4=(Y_1+Y_2).N_4+\Gamma_FN_3 \quad (17d)$$

$$N_1=(Y_1+Y_2).T-k_1C_Nb_4Y_2\theta_{FS} \quad (17e)$$

$$N_2=T.\Gamma_F \quad (17f)$$

$$N_3=(Y_1+Y_2).S-Y_1k_1C_N-\omega^2\Gamma_N\Gamma_F \quad (17g)$$

Table 3 Parameter values for Ni–Fe alloy electrodeposition

B/ T	R_S/ Ω	α	10^6 Q/IS unit	C_{dl}/ μF	R_{ct}/ Ω	I_s/ mA	$R_{ct}I_s$/ mV
0	15	0.96	26	19	43	2.04	88
0.3	16	0.95	27	19	39	2.04	80
0.6	15	0.94	32	21	36	2.1	76
0.9	15	0.93	36	21	38	1.86	71

$NiSO_4$=0.5 mol l^{-1}, $FeSO_4$=0.01 mol l^{-1}, Na_2SO_4=0.6 mol l^{-1}, H_3BO_3=0.4 mol l^{-1}, pH=3, T=25 °C. Applied potential E=−1.4 V/SSE

R_S Electrolyte resistance, α adimensional term, Q constant phase element, C_{dl} double layer capacity, R_{ct} transfer charge resistance, I_S current

Table 4 Parameter values for Ni–Fe alloy electrodeposition

B/ T	R_S/ Ω	α	10^6 Q/IS unit	C_{dl}/ μF	R_{ct}/ Ω	I_s/ mA	$R_{ct}I_s$/ mV
0	13	0.92	50	27	33	1.96	65
0.3	13	0.95	56	39	34	1.74	59
0.6	14	0.93	65	41	35	1.72	60
0.9	14	0.92	49	27	38	1.79	68

$NiSO_4$=0.5 mol l^{-1}, $FeSO_4$=0.1 mol l^{-1}, Na_2SO_4=0.6 mol l^{-1}, H_3BO_3=0.4 mol l^{-1}, pH=3, T=25 °C. Applied potential E=−1.4 V/ SSE

R_S Electrolyte resistance, α adimensional term, Q constant phase element, C_{dl} double layer capacity, R_{ct} transfer charge resistance, I_s current

$$N_4=S\Gamma_F+(Y_1+Y_2).\Gamma_N \quad (17h)$$

where:

$$S=k_1C_N+k_2\Gamma_N \text{ and } T=b_2k_2\Gamma_N\theta_{NS}-b_1k_1C_N.(1-\theta_{NS}-\theta_{FS}) \quad (18)$$

When mass transport term ($\Delta C_F/\Delta E$) can be neglected therefore the total impedance Z' can be written as:

$$Z'=R_S+Z_1/(Z_1^2+Z_2^2)-j.Z_2/(Z_1^2+Z_2^2) \quad (19)$$

where:

$$Z_1=R_{ct}^{'-1}+B_F.\mathrm{Re}(\theta_F)+B_N.\mathrm{Re}(\theta_N)+Q.\omega^{\alpha}.\cos(\alpha\pi/2) \quad (20a)$$

and

$$Z_2=\omega.[B_F.\mathrm{Im}(\theta_F)+B_N.\mathrm{Im}(\theta_N)]+Q.\omega^{\alpha}.\sin(\alpha\pi/2) \quad (20b)$$

Table 5 Experimental and calculated parameter values for different magnetic field amplitudes (same electrolytic conditions as in Table 3)

B/T	0	0.3	0.6	0.9
I_{cal}/mA	2.0	2.0	2.1	1.9
I_{exp}/mA	2.04	2.04	2.10	1.86
R'_{ctcal}/Ω	43	44	37	45
R'_{ctexp}/Ω	46	39	36	39
%Fe $_{cal}$	7.4	9.5	14.2	17.2
%Fe $_{exp}$	9.0	9.2	10.8	17.3
10^4 Y_1/mol m^2 s^{-1}	1	1.4	2.2	2.7
θ_{NS}	0.4	0.4	0.4	0.3
θ_{FS}	0.2	0.3	0.3	0.4
b_4/V^{-1}	11	25	48	31
10^4 Y_2/m^{-1} s^{-1}	1.6	2	2.8	2.2
10^4 Γ_F/mol m^{-2}	0.24	0.53	1.3	1.3

cal and *exp* stand for calculated and experimental, respectively. *I* electrolytic current, R_{ct} and R'_{ct} charge transfer resistance, *%Fe* iron amount in the deposited alloy. Y_1 and Y_2 are defined by Eqs. 8c and 8d, respectively. θ_N and θ_F are the ratios of the surface covered by $Ni(I)_{ads}$ and $Fe(I)_{ads}$, respectively. b_4 is the Tafel coefficient for step 4.

Table 6 Experimental and calculated parameter values for different magnetic field amplitudes (same electrolytic conditions as in Table 4)

B/T	0	0.3	0.6	0.9
I_{cal}/mA	2.00	1.76	1.70	1.80
I_{exp}/mA	1.96	1.74	1.72	1.79
R'_{ctcal}/Ω	36	48	52	57
R'_{ctexp}/Ω	34	35	35	39
%Fe $_{cal}$	26	57	59	62
%Fe $_{exp}$	31	58	60	62
10^3 Y_1/mol m^2 s^{-1}	0.5	1.6	1.8	2.6
θ_{NS}	0.4	0.15	0.15	0.1
θ_{FS}	0.25	0.7	0.7	0.7
b_4/V^{-1}	21	25	22	19
10^4 Y_2/m^{-1} s^{-1}	7.0	3.7	3.6	4.1
10^4 Γ_F/mol m^{-2}	0.8	4.2	3.5	2.5

cal and *exp* stand for calculated and experimental, respectively. *I* electrolytic current, R_{ct} and R'_{ct} charge transfer resistance, *%Fe* iron amount in the deposited alloy. Y_1 and Y_2 are defined by Eqs. 8c and 8d, respectively. θ_N and θ_F are the ratios of the surface covered by $Ni(I)_{ads}$ and $Fe(I)_{ads}$, respectively. b_4 is the Tafel coefficient for step 4.

Some examples of experimental EIS diagrams measured for two iron species concentration are shown in Figs. 4 and 5. The effect of the inhibiting iron species is highlighted by the very large inductive loops for middle frequency range, and the diffusion phenomenon for these same species leads to the low frequency range capacitive loop. The surface development and the hydrogen evolution thwart long measurement times, and it is not possible to get accurate results for frequency lower than 10 mHz.

Analyzing the high frequency capacitive loops, one can estimate the parameters as it was done for nickel electrodeposition from iron-free solution (Tables 3 and 4).

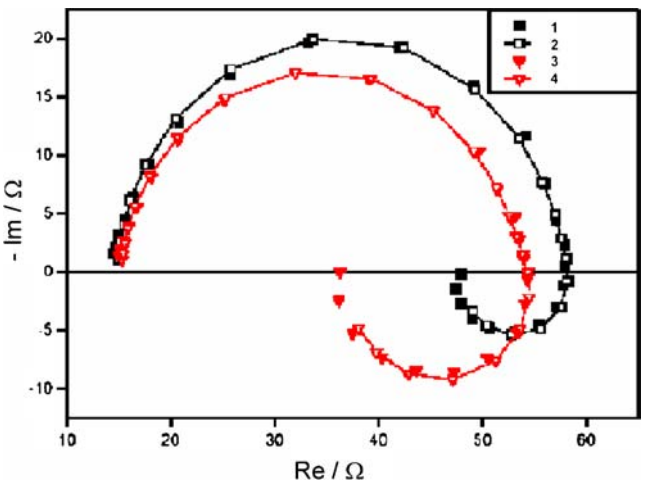

Fig. 6 Experimental (*1* and *3*) and calculated (Eq. 19; *2* and *4*) electrochemical impedance diagrams. Same electrolytic conditions as Fig. 4. B=0 for diagrams *1* and *2*. B=0.9 T for diagrams *3* and *4*

Because the charge transfer resistance depends on the covered surface ratios (Eq. 14) and therefore on the diffusion layer thickness (Eq. 8a–c, and d), it is not possible to conclude on the magnetic field effect on charge transfer steps as for simple nickel case.

Taking into account the inductive loops that are dependent on the iron species diffusion process, it is possible to determine all the parameters that are involved in the electrodeposition process and that lead to the stationary and dynamic expressions (Eqs. 7 and 19).

These calculations were undertaken by the same regression method than for nickel case. Moreover, a comparison between experimental values of stationary currents and atomic iron amounts in the deposit and the values that can be recalculated with parameters derived from the impedance diagram analyses was included in the fitting software. That method and the parameter values obtained before with nickel electrodeposition analysis allowed a statistical determination of the R'_{ct}, Y_1, Y_2, Γ_F and b_4 values (Tables 5 and 6) with standard errors less than 5%.

For the lowest iron concentration, the model fits very well the experimental diagrams (Fig. 6), and the determined parameter values are in a very good accordance with the experimental ones (Table 5). For low frequencies (frequency $\leq$ 0.05 Hz), the EIS calculated data do not match the experimental ones for higher iron concentration and high magnetic fields. In fact, a Warburg impedance term has to be added to fill up the model, which is not possible due to the lack of precision on the low frequency data. Nevertheless, the two tables (Tables 5 and 6) show that the magnetic field has no effect on the iron charge transfer process. Indeed, for a constant iron concentration, the Y_2 ($Y_2 = k_4.\Gamma_F$) term keeps a constant value for any no zero magnetic field amplitude. That is more particularly true when the iron current percentage is higher due to a high iron species concentration and an effective magnetic convective effect. Moreover, the Y_2 value that is obtained for high iron concentration, and no magnetic field has to be disregarded because in this case, the natural convection does not allow an actual accurate determination. Finally, an average Tafel coefficient can be estimated as b_4=28 V^{-1}, which is comparable to previous results [10, 11]. For the Y_1 term, which represents the convective diffusion process induced by the magnetic field (Y_1 is the iron species flux at the electrode), three points may be highlighted. The first one is that no iron concentration effect is noticeable on the diffusion layer thickness when the magnetic field is superimposed. This result is coherent with a Lorentz force effect and the total current that is quite constant for this applied potential. The second one is the lack of precision that has been mentioned above, which prevents any correct determination for the relationship between magnetic field amplitude and diffusion layer thickness. Further investigations have to be undertaken specially by means of MHD transfer function analyses [23], which could supply more precise data and opportunities for parameter determinations. The last remark concerns the amplitude of the bulk concentration of the electroactive iron species: With a superimposed magnetic field as used in our experiments, a typical order of the diffusion layer thickness is in the order of some dozens of micrometers. Therefore, the C_F can be estimated in about ten times less than the Fe^{2+} concentration, which is much more than the hydroxyl $Fe(OH)^+$ [9]. We find for iron ion reduction the same conclusion than for Ni(II) reduction mechanism. Therefore, the reactive species at the electrode cannot be the hydrolyzed metal ions, which have a too low bulk concentration. This conclusion is in accordance with [14, 15], which concluded that a hydroxide-based model cannot explain the NiFe alloy codeposition.

Conclusion

Iron nickel alloy electrodeposition has been realized with different superimposed magnetic fields. For a horizontal downward electrode in a homogeneous, constant, horizontal magnetic field, stationary and dynamical analyses lead to determine the mechanism parameters of the electrochemical reactions. The magneto-induced convection decreases the diffusion layer thickness and consequently controls the iron amount in the deposit. The values of the kinetic parameters that can be obtained do not support mechanism with hydroxyl intermediates. Finally, the magnetic field does not provoke a noticeable modification on the charge transfer process.

References

1. Msellak K, Chopart J-P, Jbara O, Aaboubi O, Amblard J (2003) Magnetohydrodynamics 39:487–493
2. Msellak K, Chopart J-P, Jbara O, Aaboubi O, Amblard J (2004) J Magn Magn Mater 281:295–304
3. Devos O, Aaboubi O, Chopart J-P, Olivier A, Merienne E, Amblard J (1998) J Electrochem Soc 145:4135–4139
4. Fahidy TZ (2001) Progr Surf Sci 68:155–188
5. Brenner A (1963) Electrodeposition of alloys. Principles and practice. Academic, New York
6. Landolt D (1994) Electrochim Acta 39:1075–1090
7. Landolt D, Podlaha EJ, Zech N (1999) Z Phys Chem 208:167–182
8. Dahms H, Croll IM (1965) J Electrochem Soc 112:771–775
9. Hessami S, Tobias CW (1989) J Electrochem Soc 136:3611–3616
10. Matlosz M (1993) J Electrochem Soc 140:2272–2279
11. Baker BC, West AC (1997) J Electrochem Soc 144:169–175
12. Zech N, Podlaha EJ, Landolt D (1999) J Electrochem Soc 146:2886–2891
13. Zech N, Podlaha EJ, Landolt D (1999) J Electrochem Soc 146:2892–2900
14. Vaes J, Fransaer J, Celis J-P (2000) J Electrochem Soc 147:3718–3724

15. Vaes J, Fransaer J, Celis J-P (2002) J Electrochem Soc 149:C567–C572
16. Devos O, Olivier A, Chopart J-P, Aaboubi O, Maurin G (1998) J Electrochem Soc 145:401–405
17. Devos O, Aaboubi O, Chopart J-P, Olivier A, Gabrielli C, Tribollet B (2000) J Phys Chem A 104:1544–1548
18. Aaboubi O, Amblard J, Chopart J-P, Olivier A (2001) J Phys Chem B 105:7205–7210
19. Wiart R (1968) Oberflache Surface 9:213–291
20. Chopart J-P, Douglade J, Fricoteaux P, Olivier A (1991) Electrochim Acta 36:459–463
21. Koehler S, Bund A (2006) J Phys Chem B 110:1485–1489
22. Brug GJ, Van Den Eeden ALG, Sluyters-Rehbach M, Sluyters JH (1984) J Electroanal Chem 176:275–295
23. Devos O, Aaboubi O, Chopart J-P, Merienne E, Olivier A (1999) Electrochemistry 67:180–187